Biosensors and Bioelectronics 198 (2022) 113830

Contents lists available at ScienceDirect

Biosensors and Bioelectronics

journal homepage: www.elsevier.com/locate/bios

Rapid detection of miRNA via development of consecutive adenines (polyA)-based electrochemical biosensors

Xiaoyu Hua [a], Jingjing Fan [a], Lingzhi Yang [b,**], Jun Wang [d], Yongqiang Wen [a], Lei Su [c,*], Xueji Zhang [c]

[a] School of Chemistry and Biological Engineering, University of Science and Technology Beijing, Beijing, 100083, PR China
[b] School of Pharmaceutical Sciences, Health Science Center, Shenzhen University, Shenzhen, 518037, PR China
[c] School of Biomedical Engineering, Health Science Center, Shenzhen University, Shenzhen, 518037, PR China
[d] Department of Biomedicine and Biopharmacology, Hubei University of Technology, Wuhan, 430068, PR China

ARTICLE INFO

Keywords:
Electrochemical DNA biosensors
Rapid detection
polyA
LAMP
miRNA analysis

ABSTRACT

Herein, we report rapid electrochemical detection of miRNA let-7a based on a DNA probe consisting of a polyA and Fc-*co*-labeled harpin structure (the polyA-H probe). The polyA-H probe could be facilely immobilized on Au surfaces through the interactions between polyA and Au, followed by its pre-hybridization with a single strand (S1). The probe's surface density could be optimized for minimizing steric hindrance via changing the polyA block length. The target let-7a could be rapidly amplified via loop-mediated isothermal amplification (LAMP) with four simplified primers, followed by inducing the formation of dimeric i-motif (DIM) structure via H^+-induced rapid folding of two C-rich sequences of motif strand 1 and strand 2. It was found that, after introducing the as-formed DIM to hybridize the S1, the immobilized $polyA_{20}$-H probe could rapidly revert to its hairpin structure, sending out a turn-on electrochemical signal of the Fc. The total time for detecting the let-7a was around 80 min, obviously less than that of most of electrochemical DNA sensors reported previously. The biosensor showed a linear relationship of the current response to the let-7a in the range of 10 fM to 50 nM with a limit of detection (LOD) of 5.1 fM. Our biosensors were further tested using human serum spiked with the let-7a and the extracts of the breast adenocarcinoma cells spiked with and without the let-7a, respectively. Satisfied results were obtained. This study shows a potential promising future of development of electrochemical biosensors for rapid detection of miRNAs in the application of clinical practice.

1. Introduction

In clinical practice, rapid detection of disease biomarkers is highly desirable, because it can shorten the waiting time for diagnosis, facilitating patients to be timely admitted to hospital and to receive timely and early medical treatment (Hu et al., 2017; Jing et al., 2019; Zhang et al., 2020). Especially in the emergency cases, rapid detection of disease biomarkers can facilitate timely diagnosis for providing urgent and effective treatments, avoiding irretrievable acute pathophysiological injuries (Hu et al., 2021; Kelley, 2017; Xiao et al., 2017). In recent years, miRNAs have been widely considered as an essential and effective biomarker for disease diagnosis, pathological analysis, and prognosis evaluation (Gai et al., 2020; Zhou et al., 2021). Consequently, many methods have been proposed to meet the needs of clinical rapid detection of miRNAs, such as fluorescent (Wang et al., 2016; Ying et al., 2018), chemiluminescent (Shi et al., 2019), colorimetric (Zhou et al., 2021), and electrochemical methods (Shi et al., 2018; Xue et al., 2021; Zouari et al., 2020b). Among these methodologies, electrochemical methods possess the irresistibly attractive advantages of technological functionality and commercial applications such as high response sensitivity, low cost, convenient operation, and ease of miniaturization, integration and portability, making it a promising future for miRNA detection applications. However, currently, they have been in an embarrassing situation in miRNA detection applications, mainly due to their weakness in the ability of rapid miRNA detection. In other words, currently, the bottleneck problem of electrochemical miRNA detection is that electrochemical detection is time consuming, usually more than 150 min, making electrochemical methods almost completely

* Corresponding author.
** Corresponding author.
E-mail addresses: yanglingzhi@szu.edu.cn (L. Yang), sulei@szu.edu.cn (L. Su).

https://doi.org/10.1016/j.bios.2021.113830
Received 3 October 2021; Received in revised form 11 November 2021; Accepted 19 November 2021
Available online 26 November 2021

uncompetitive for rapid miRNA detection applications. Therefore, it is of great scientific and technological significance to develop effective strategies for rapid electrochemical detection of miRNAs. Recently, a few progresses have been made in this direction. For instance, Raouafi group reported a new electrochemical biosensor to detect the target miRNA in a single 30-min incubation step (Zouari et al., 2020a).

Usually, electrochemical detection of miRNAs is based on DNA probe recognition-induced hybridization with target miRNAs on electrode surfaces followed by the signal conversion into electrochemical response (Azzouzi et al., 2019; Ferapontova et al., 2008). Such a DNA-based biorecognition and the subsequent signal conversion are highly dependent on the interface states of the self-assembled monolayer (SAM) of DNA probes formed on electrode surfaces (Somasundaram and Easley, 2019). Rational control of the interface states of the SAM of DNA probes, especially the control of the DNA probe density and minimization of steric hindrance effects, however, remains great challenging. For instance, generally, the most common and simple strategy for constructing a DNA probe interface is to use the DNA oligonucleotide sequence tagged with a thiol (-SH) group for directly anchoring on gold electrode surfaces (Pei et al., 2012). Nevertheless, it has been found to be difficult to accurately control the density, orientation, and distance of DNA strands through the Au–S bond (Pei et al., 2012). Due to the presence of relatively large steric hindrance effects (Zhu et al., 2016), the process of the DNA probe's recognition and hybridization with target miRNA occurring on electrode surfaces as well as the subsequent signal conversion is obviously sluggish, comparative with that occurring in aqueous solutions.

Recently, a novel DNA probe immobilization approach based on the thiol-free polyA-Au interaction has emerged as an alternative to the traditional –SH–tagged DNA probes (Hu et al., 2020; Pei et al., 2012; Zhang et al., 2018). PolyA can stick to gold surfaces with high affinity via hydrophobic collapse in the adhesion process, hence the DNA probe tagged with polyA can be facilely immobilized on gold surfaces (Hu et al., 2020; Pei et al., 2012; Zhu et al., 2016). More importantly, by simply adjusting the length of the polyA, the lateral spacing and surface density of DNA on gold surfaces can be programmably tuned, which was otherwise difficult to achieve with thiolated DNA (Li et al., 2018; Yang et al., 2018). Such a polyA strategy has brought several important and innovative progresses in the field of DNA sensors including one-step immobilization of antibodies and DNA probe, the enhancement of motion efficiency of the three-dimensional DNA motor, and the improvement of the sensing sensitivity of electrochemical DNA sensors (Li et al., 2018). However, such an elegant polyA strategy has not yet exhibited its great value in the field of rapid electrochemical nucleic acid detection.

Herein, we report the rapid electrochemical biosensing of miRNA let-7a based on the let-7a-involved LAMP and the turn-on type polyA based DNA probe. The let-7a can negatively regulate the expression of Ras oncogenes and display decreased expression in various cancers such as breast cancer and lung cancer (Chen et al., 2018; Zhang et al., 2021). It is known that in nucleic acid detection, nucleic acid amplification treatment such as polymerase chain reaction (PCR), strand displacement amplification (SDA), hybridization chain reaction (HCR) and LAMP is essential and necessary (Chai et al., 2021; Miao and Tang, 2021). LAMP can amplify DNA with high specificity, efficiency and rapidity under isothermal conditions (Wu et al., 2020). In this study, the miRNA let-7a involved LAMP utilized four simplified primers, template of stem-loop DNA (TD), loop DNA (LD), forward primer (FP), and backward primer (BP), which could enhance the generation efficiency of the double stem-loop DNAs, reducing the amplification time. The polyA-based DNA probe was designed to consist of a polyA end, a harpin structure with redox Fc at the other end. With the aid of the polyA end, the probe could be facilely immobilized on the electrode surface and the surface density of the $polyA_{20}$-H could be precisely controlled by varying the length of the polyA block. Accordingly, the steric hindrance effects could be reduced obviously, accelerating the process of the DNA probe's recognition and hybridization with the target well as the subsequent signal conversion. Subsequently, compared with most of previous studies, more rapid electrochemical detection of target miRNA (around 80 min) can be achieved.

2. Experimental

2.1. Reagents and chemicals

Chloroauric acid ($HAuCl_4{\cdot}4H_2O$) and 6-mercapto-1-hexanol (MCH) were obtained from Beijing Huawei Ruike Chemical Co., Ltd. (Beijing, China). Bacillus stearothermophilus 2.0 WarmStart DNA polymerase (Bst) and 10 × isothermal amplification buffer were supplied by New England Biolabs Ltd. (Beijing, China). Human real serum sample was obtained from Lablead Biotech Co., Ltd. (Beijing, China). Deoxynucleotide triphosphates (dNTPs), DNA marker (25–500 bp), 1X TE buffer, DEPC-treated water, and oligonucleotides were provided by Sangon Biotech Co. Ltd (Shanghai, China). The detailed base sequences of all oligonucleotides are listed in Table S1. Other chemicals of at least analytical purity were purchased from Beijing Chemical Corporation (Beijing, China). The ultrapure water used throughout this study was obtained from a Millipore water purification system (≥18 MΩ, Milli-Q, Millipore, USA).

2.2. Target miRNA let-7a-triggered LAMP reaction

Different oligonucleotides for LAMP reaction were dissolved separately in 1 × TE buffer to prepare the storage solution with a final concentration of 100 μM, which were further diluted with the DEPC-treated water when in use. Firstly, 0.2 μM TD, 0.2 μM LD, 1 × isothermal amplification buffer, 12 U Bst, 1.0 mM dNTPs and different concentrations of target let-7a were mixed with a final volume of 12.0 μL. Then, the mixture solution reacted in a heating incubator at 50 °C for 10 min. Next, the other solution of 8.0 μL containing 2.0 μM backward primer (BP), 2.0 μM forward primer (FP), 0.5 M betaine, 5.0 mM NH_4Cl and 10.0 mM $MgSO_4$ was added to the above mixture solution. Subsequently, the resultant mixture solution was kept at 65 °C to perform LAMP reaction for 30 min, followed by naturally cooling down to room temperature. 1 μL of motif strand 1 (M1) (40 μM) and 1 μL of motif stand 2 (M2) (40 μM) were introduced into the final solution to form the DIM structure.

2.3. Fabrication of the electrochemical DNA biosensors

Firstly, the $polyA_{20}$-H probe (1 μM) hybridized with the single strand S1 (1 μM) were incubated with the cleaned Au electrodes overnight, which was denoted as the $polyA_{20}$-H:S1 electrode. Then, MCH (0.1 mM) was used to modify the electrode for 30 min. Afterwards, 10 μL of the DIM was introduced to hybridize with the S1 of the $polyA_{20}$-H:S1 probe for 40 min, to restore the hairpin structure of the $polyA_{20}$-H. It was noted that each step of the electrode modification was followed by washing with Tris-HCl buffer solution.

2.4. Polyacrylamide gel electrophoresis (PAGE)

The LAMP products were characterized with the 8% freshly prepared non-denaturing polyacrylamide gel. Briefly, 10 μL of each sample was mixed with 2 μL of 6 × loading DNA buffer and then added to the nondenaturing polyacrylamide gel. The electrophoresis was performed at 120 V for 50 min in 1 × TBE buffer. Finally, the electrophoresis was imaged under the UV light illumination after stained with Gel Red.

2.5. Apparatus

Cyclic voltammetry (CV) and square wave voltammetry (SWV) were performed on a CHI 852C electrochemistry workstation (CH Instruments Inc., Shanghai, China) equipped with a conventional three-electrode

system with an Au substrate electrode (3 mm in diameter) as the working electrode, a platinum wire as auxiliary electrode and an Ag/AgCl reference electrode. Fluorescence spectrum was measured on a Hitachi F-4500 fluorescence spectrofluorometer (Tokyo, Japan). DIM structure was characterized using a CD spectrophotometer (JASCO J-1500). UV–vis absorption spectrum was measured with a UV-6100S spectrometer (Mapada, China).

3. Results and discussion

3.1. Design of rapid electrochemical biosensing of miRNA let-7a

As shown in Scheme 1, as the introduction of the miRNA let-7a, four simplified primers, TD, LD, FP and BP under the help of Bst and dNTPs, start the LAMP, generating a certain amount of H^+ to induce the folding of two C-rich sequences M1 and M2 to form the DIM structure working as signal transducer. The electrode surfaces are modified with the Fc-labeled polyA$_{20}$-H, which is further hybridized with the S1 to render the probe upright. The unpaired overhangs of the DIM can hybridize with the S1, resulting in the dehybridization of the polyA$_{20}$-H probe, thereby reverting to its hairpin structure. As a result, the Fc group can approach close to the Au surface, leading to the increase in the electrochemical signal, which can be utilized to quantify the target miRNA let-7a.

3.2. Characterizations of the miRNA let-7a-involved LAMP and the formation of the DIM

The PAGE and fluorescence images of the LAMP products with different concentrations of the let-7a are shown in Fig. 1A and B, respectively. From Fig. 1A, the characteristic ladder-like multiple bands could be observed, which can be attributed to the double-stranded DNA products of the target let-7a-induced LAMP. From Fig. 1B, in the absence of the let-7a, the observed fluorescence of the SYBR Green I was weak, while in the presence of the let-7a, the observed fluorescence was greatly enhanced; moreover, with the increase of the let-7a concentration, the observed fluorescence intensity was increased. These observations indicate the generation of the double-stranded DNA by the let-7a-induced LAMP. Accordingly, it was found that the LAMP reaction resulted in a gradual decrease of the pH value of the reaction solution, corresponding to the release of H^+ from the let-7a-involved LAMP. Owing to the use of the simplified primers, the total time of the let-7a-involved LAMP reaction was measured to be around 40 min, much less than the time required for conventional nucleic acid amplification methods.

Fig. 1C shows the CD spectra of the formed DIM. It can be seen that the CD curves have a negative peak near 255 nm and a strong positive peak near 285 nm, corresponding to the specific absorptions of the i-motifs in the CD spectra (Nesterova and Nesterov, 2014), confirming the formation of the DIM. The formation of the DIM could also be indicated by fluorescent label method with the aid of the modification of the M1 and the M2 with a black-hole quencher (M1$_{BHQ1}$) and a fluorophore (M2$_{FAM}$), respectively. As schematically illustrated by Scheme S1, in the neutral solution, M1$_{BHQ1}$ in the free state does not affect the fluorescence of the M2$_{FAM}$ in the free state, while in the acidic solution, the M1$_{BHQ1}$ can assemble spontaneously with the M2$_{FAM}$ to form the DIM structure, resulting in the fluorescent FAM group approaching close to the BHQ1 and being quenched by the latter. As shown in Fig. S1, in the solution of the target let-7a-induced LAMP reaction products, the fluorescence emission intensity of the M2$_{FAM}$ decreased, indicating the formation of the DIM structure.

3.3. Stepwise electrochemical characterizations of the electrochemical biosensor

As shown in Fig. 2A, after immobilizing the polyA$_{20}$-H:S1 at the bare Au substrate, in blank PBS, the SWV response was observed to increase (curve b). After further introduction of the DIM, an obvious increase in the SWV response was observed (curve c), indicating the dehybridized polyA$_{20}$-H reverting to its hairpin structure, leading to the Fc group

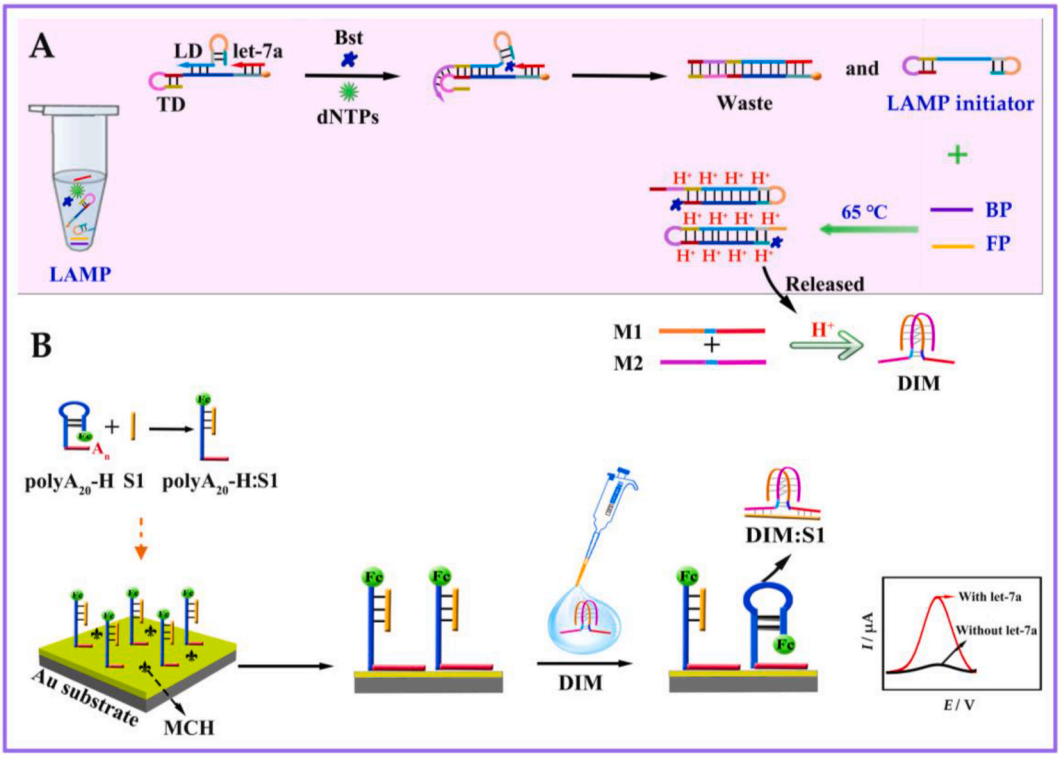

Scheme 1. Schematic diagrams of (A) the target miRNA Let-7a triggered-LAMP with four simplified primers and (B) the formation of DIM from the H^+-induced folding of M1 and M2, and the polyA$_{20}$-H-based electrochemical sensing.

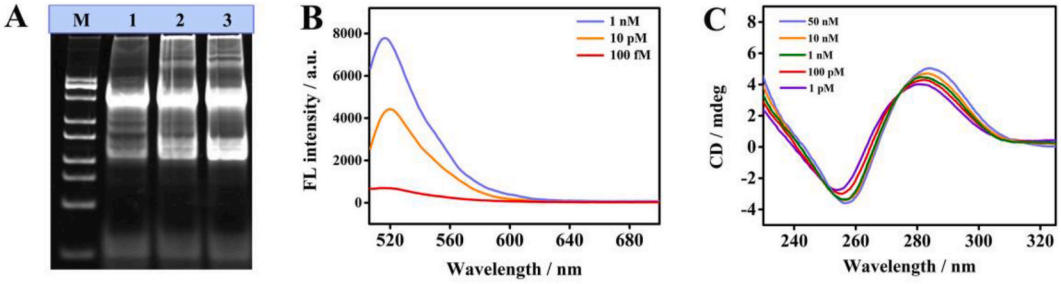

Fig. 1. (A) PAGE image of the DNA products of the LAMP reaction in the presence of different concentrations of let-7a (100 fM, lane 1; 10 pM, lane 2; 1 nM, lane 3). Lane M is DNA-marker: 25–500 bp (25, 50, 75, 100, 150, 200, 300, 400 and 500 bp, from the bottom to the top). (B) Fluorescence response of SYBR Green I to the DNA products of the LAMP in the presence of different concentrations of the let-7a. (C) CD spectra of the different concentration of the DIM corresponding to different concentrations of the let-7a. (For interpretation of the references to color in this figure legend, the reader is referred to the Web version of this article.)

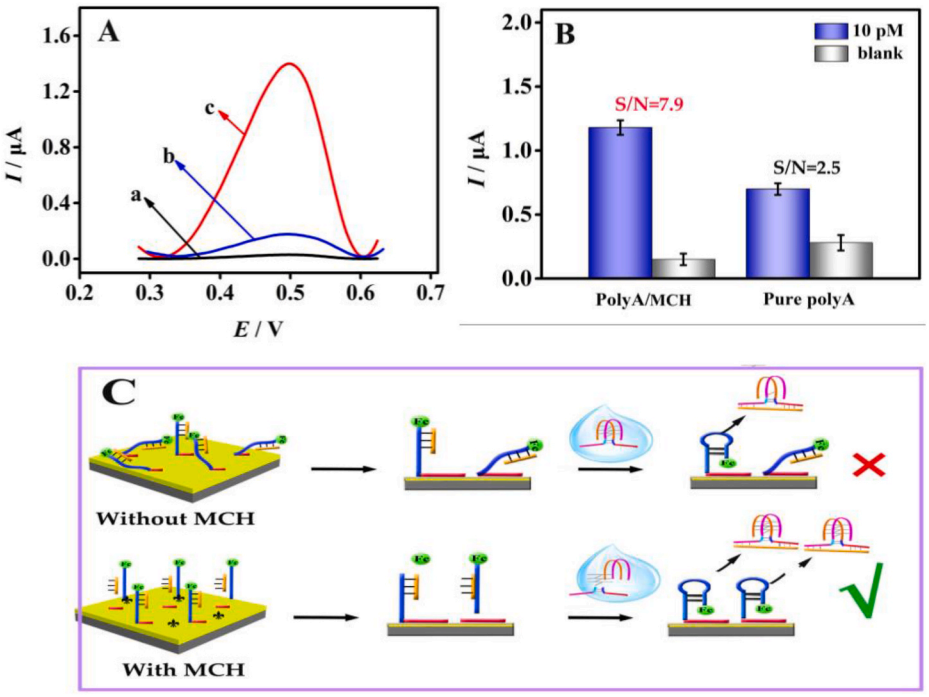

Fig. 2. (A) SWV response of different modified electrodes: (a) the bare Au substrate, (b) the polyA$_{20}$-H:S1/Au, and (c) the DIM/polyA$_{20}$-H:S1/Au. Scan rate: 0.1 V s^{-1}. The concentration of the let-7a for the LAMP was 10 pM. (B) SWV peak current response of the Fc group of the polyA$_{20}$-H:S1 electrodes with and without the MCH modification to the target let-7a. (C) Schematic illustration of the effect of MCH modification on the electrochemical detection.

approaching close to the substrate electrode surfaces, thereby increasing the SWV response of the Fc group. These results noted that the as-prepared electrochemical biosensors were capable of detecting the target miRNA let-7a.

The effect of MCH modification on the response of the polyA$_{20}$-H:S1/Au electrode to the target let-7a was further studied. As shown in Fig. 2B, a better signal to noise ratio (S/N) for the let-7a was obtained at the polyA$_{20}$-H/MCH electrode, compared with the polyA$_{20}$-H electrode, indicating that the MCH modification of the polyA$_{20}$-H electrode could improve the detection sensitivity. It could be associated that the adsorption of the MCH at the polyA$_{20}$-H-modified Au surfaces could help to keep the polyA$_{20}$-H upright, favorable for the interactions between the polyA$_{20}$-H:S1 chain and the DIM to dehybridize the polyA$_{20}$-H reverting to its hairpin structure, as shown in Fig. 2C.

3.4. Optimization of the polyA block length

The surface density of the probe can be conveniently controlled by changing the length of the polyA block (A$_{10}$, A$_{20}$, and A$_{30}$). The assembling density (Γ) of the different SAMs including the polyA$_n$-H:S1 (n = 10, 20, and 30) were investigated with chronocoulometry in 10 mM Tris-HCl (pH 7.4) in the absence and presence of RuHex (50 μM) as electron mediator, respectively. The Γ could be calculated via the equation $\Gamma = [(Q_{ss}N_A)/(nFA)](z/m)$, where N_A was the Avogadro constant, n was the number of electron transferred, F was the Faraday constant, m was the number of nucleotides in the DNA and z was the charge of the redox molecule. Fig. S2 shows the relationship between the charges (Q) and the square root of scan time ($t^{1/2}$). Two intercepts at t = 0 was related to the total charge with RuHex (Q_{total}) and the double layer charge without RuHex (Q_{dl}), respectively. Therefore, the charge corresponding to RuHex electrostatically bound to the surface-confined DNA (Q_{ss}) = Q_{total}-Q_{dl} could be obtained. The electroactive surface area A was obtained by measuring the CV response in 5 mM $[Fe(CN)_6]^{3-/4-}$ solution at different scan rates from 0.03 to 0.21 V s^{-1}, as shown in Fig. S3, and the A was calculated to be 14.28 mm^2 (see the caption of Fig. S3). So, the density of the polyA$_{10}$-H:S1, polyA$_{20}$-H:S1, and polyA$_{30}$-H:S1 on the electrode surfaces was 4.1 × 10^{12} molecules cm^{-2}, 2.1 × 10^{12} molecules cm^{-2} and 1.3 × 10^{12} molecules cm^{-2}, respectively (Fig. 3A). Obviously,

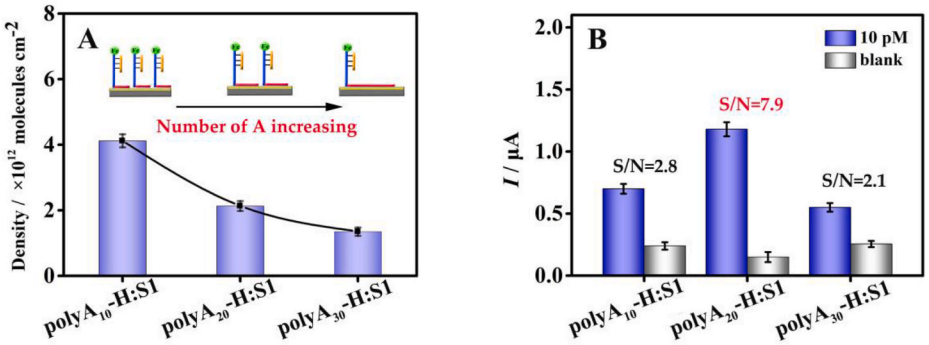

Fig. 3. (A) The densities (Γ) vs the length of the polyA block. (B) SWV peak current responses of the Fc group of the polyA$_n$-H:S1 with different lengths of the polyA block (n = 10, 20, and 30) in the absence and presence of let-7a, respectively. The concentration of let-7a was 10 pM. Error bars: standard deviation (s), n = 3.

the reduction ratio in surface density was almost consistent with the increase ratio in the polyA block length, indicating that all A bases in the polyA block completely covered the electrode surface; and, the increase in the length of the polyA block (from the polyA$_{10}$-H to the polyA$_{30}$-H) indicates the increase in the inter-strand spacing the probe on the electrode surface, resulting in the decrease in the assembling density. Furthermore, as shown in Fig. 3B, it can be found that the highest S/N was obtained for the polyA$_{20}$-H:S1, indicating that the polyA$_{20}$ could properly reduce the DNA probe's surface density and thus increase the inter-strand spacing to reduce steric hindrance, promoting the hybridization ability and the formation of its hairpin structure.

3.5. Time optimization of the incubation of probe

As shown in Fig. 4A, obviously, as the DIM was introduced, the SWV response of the Fc group gradually increased and reached a plateau after 40 min, indicating that 40 min was sufficient for the polyA$_{20}$-H to revert to its hairpin structure and to send out the electrochemical signal. In addition, the fluorescent method was utilized as a complementary method to evaluate approximately the incubation time of the DIM with the probe. To this end, a hairpin labeled with the fluorophore FAM tags (polyA$_{20}$-H$_{FAM}$) was designed and the resultant polyA$_{20}$-H$_{FAM}$:S1 were attached onto the surfaces of 12-nm-diameter AuNPs (Fig. S4). Then, the DIM formed by the let-7a-induced LAMP led to the dehybridization of the polyA$_{20}$-H$_{FAM}$/AuNPs reverting to its hairpin structure, accompanied with the FAM tags approaching to the AuNPs, resulting in the fluorescence quenching of the FAM. As shown in Fig. S5, with the incubation time increasing to 40 min, the fluorescence intensity gradually decreased and levelled off, suggesting that the polyA$_{20}$-H$_{FAM}$ dehybridized and reverted to its hairpin structure after 40 min, consistent with the aforementioned SWV results. For contrast, the DNA hairpin tagged with the SH (SH–H) was used to hybridized with the S1 (SH–H:S1). As shown in Fig. 4B, the SWV response of the Fc group could not level off only until 100 min. Therefore, the total time for the detection process (viz., the time of the LAMP treatment of the samples plus the time for the electrochemical detection) was within 80 min, obviously less than most of previous reports (References S1), as shown in Fig. 4C.

3.6. Sensing performance

As shown in Fig. 5A, with the increase in the concentration of the let-7a, the SWV response of the Fc group gradually increased. The resultant calibration curve was plotted with the SWV peak current ΔI (ΔI=I–I_0, where I_0 was the background signal) versus the logarithm of the let-7a concentrations in the range of 10 fM to 50 nM (Fig. 5B). Obviously, a good linear relationship was obtained with a corresponding linear equation of $\Delta I = 0.3288\lg c_{let\text{-}7a} + 1.6792$ and a correlation coefficient $r = 0.9958$. According to IUPAC definition (Long and Winefordner, 1983), the LOD was calculated by the equation $I = I_0 + 3s_B$, where I_0 and s_B are the SWV signal and the standard deviation of the blank sample, respectively. As a result, the LOD was calculated to be 5.1 fM. Moreover, compared with some previous reports as listed in Table S2, our sensor achieved wide linear range and low LOD for let-7a detection.

3.7. Specificity, reproducibility, and stability

To assess the specificity of the as-prepared electrochemical biosensor, other let-7 family members (let-7b, let-7c and let-7i) at 10-fold concentration were used as interfering substances (Fig. 5C). It was found that none of them caused significant electrochemical response, indicating that the as-prepared electrochemical biosensor exhibited excellent current response specificity to the let-7a. From Fig. 5D and E, five measurements by using a biosensor (viz., the intra-assay) and five measurements by using five biosensors prepared in the same batch (viz., the inter-assay) presented almost the same SWV signal with 1.9% and 2.2% RSD, respectively, indicating a good reproducibility of the as-prepared electrochemical biosensors. To evaluate the storage stability of the as-prepared electrochemical biosensor, five biosensors

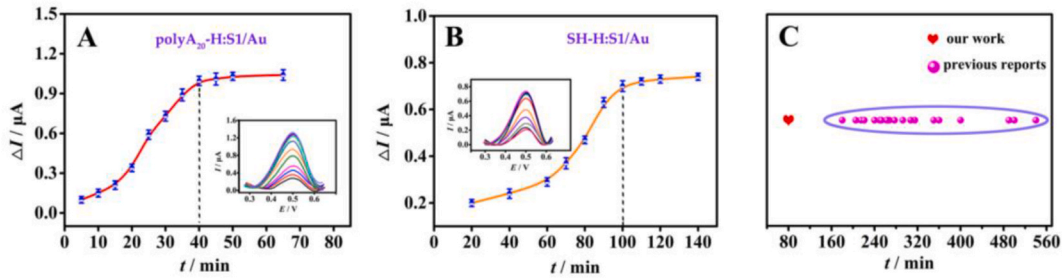

Fig. 4. SWV response of the polyA$_{20}$-H:S1 modified electrode (A) and the SH-H:S1 modified electrode (B) after incubation with the DIM for different time. The concentration of let-7a was 10 pM. Error bars: s, n = 3. (C) Comparison of the nucleic acid detection time in our work with previous reports. The time is the sum of the time for the nucleic acid amplification plus the time for the electrochemical detection.

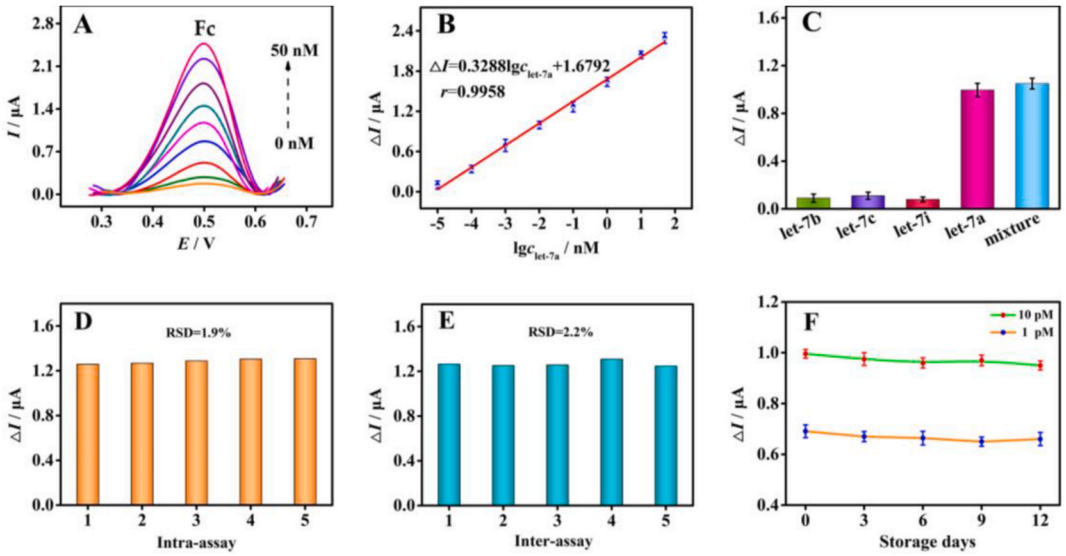

Fig. 5. (A) SWV response of the biosensor to different concentrations of the let-7a (0, 10, 100 fM, 1, 10, 100 pM, 1, 10, and 50 nM). (B) The linear calibration curve plotted by Δ*I vs.* the logarithm of the let-7a concentration. (C) Specificity of the biosensor with the let-7a (10 pM) against the let-7b (100 pM), the let-7c (100 pM), the let-7i (100 pM), and their mixture. (D) Reproducibility of five electrodes prepared in the same batch (inter-assay) and (E) five batches (intra-assay). (F) Stability of the biosensor with 1 pM and 10 pM let-7a after stored 3, 6, 9 and 12 days at 4 °C. Error bars: *s*, $n = 3$.

were stored for 3, 6, 9 and 12 days, respectively. Then, the SWV responses were obtained and found to be very stable with only slight current attenuation (less than 6% and 8%, respectively), as shown in Fig. 5F, indicating a robust stability of our biosensor.

3.8. Application of the proposed biosensor in real samples

To demonstrate the preliminary practicability and reliability of this biosensor, human serum as real biological samples were conveniently used for target let-7a detection by standard addition method (SAM). Specially, serum samples were treated with RNase inhibitor so that endogenous miRNAs were depleted before recovery experiments. Five concentrations of the let-7a (0.01, 0.05, 0.1, 1, and 5 nM) spiked into the human serum were tested by using our developed biosensor, respectively. As shown in Table S3, the recovery percentages were from 92% to 110% with relative standard deviation (RSD) in the range of 2.3–4.8%. Otherwise, the let-7a extracts obtained from the breast adenocarcinoma cells (MCF-7) (cell number 1×10^5) were served as the model miRNA target to investigate the applicability of our biosensors. As shown in Table S4, the MCF-7 was found to contain an average 0.62 nM let-7a. In addition, 2 nM let-7a was added to three extracts to perform the recovery experiment, and the obtained recoveries were ranged from 97 to 109% with the RSD in the range of 2.2–4.9%, as shown in Table S4. These results confirmed the accuracy of the biosensor developed.

4. Conclusions

In conclusion, we have demonstrated a rapid electrochemical method for sensing of miRNA let-7a based on the let-7a-involved LAMP and the turn-on type polyA-based DNA probe. The let-7a-involved LAMP utilized four simplified primers to enhance the generation efficiency of the double stem-loop DNAs, reducing the amplification time to be around 40 min. The LAMP also induced the rapid formation of the DIM as signal translator. The $polyA_{20}$-H:S1 probe could be facilely immobilized on Au electrodes via the spontaneous interactions between the polyA and Au, constructing an electrochemical biosensor for detecting the let-7a. The probe's surface density could be conveniently controlled by changing the length of the polyA block (A_{10}, A_{20}, and A_{30}), and the highest S/N was obtained for the $polyA_{20}$-H:S1. More importantly, it was found that 40 min was sufficient for the $polyA_{20}$-H probe to be dehybridized and revert to its hairpin structure, sending out the turn-on electrochemical signal. Therefore, the total time for the detection process (viz., the time of the LAMP treatment of the samples plus the time for the electrochemical detection) was within 80 min, obviously less than most of previous reports. The as-constructed electrochemical biosensor showed a linear relationship of the current response to the let-7a in the range of 10 fM to 50 nM with a LOD of 5.1 fM. The as-constructed electrochemical biosensor showed high selectivity, good reproducibility and good storage stability. Finally, human serum spiked with the let-7a and the let-7a extracts obtained from the MCF-7 were served as real biological samples were tested with our biosensors. Satisfied recovery percentages were obtained. This study shows a promising future of development of electrochemical biosensors for rapid detection of miRNAs in the application of clinical practice.

CRediT authorship contribution statement

Xiaoyu Hua: Conceptualization, Methodology, Validation, Formal analysis, Investigation, Writing – original draft. **Jingjing Fan:** Investigation, Validation. **Lingzhi Yang:** Methodology, Validation, Writing – review & editing. **Jun Wang:** Formal analysis, and. **Yongqiang Wen:** Formal analysis. **Lei Su:** Conceptualization, Methodology, Validation, Writing – review & editing, Project administration, Funding acquisition, and. **Xueji Zhang:** Project administration, Funding acquisition.

Declaration of competing interest

The authors declare that they have no known competing financial interests or personal relationships that could have appeared to influence the work reported in this paper.

Acknowledgments

We are grateful for the financial support from the National Natural Science Foundation of China, China (grant nos. 21727815, 21890740 and 21890742); Guangdong Basic and Applied Basic Research Foundation, China (2021A1515012332); National Natural Science Foundation of China, TUBITAK (Turkey)-NSFC (China) Bilateral Cooperation Program (82061138005), China; SZU Top Ranking Project, China (86000000210).

Appendix A. Supplementary data

Supplementary data to this article can be found online at https://doi.org/10.1016/j.bios.2021.113830.

References

Azzouzi, S., Fredj, Z., Turner, A.P., Ali, M.B., Mak, W.C., 2019. ACS Sens. 4, 326–334.
Chai, H., Cheng, W., Jin, D., Miao, P., 2021. ACS Appl. Mater. Interfaces 13, 38931–38946.
Chen, J., An, T., Ma, Y., Situ, B., Chen, D., Xu, Y., Zhang, L., Dai, Z., Zou, X., 2018. Anal. Chem. 90, 859–865.
Ferapontova, E.E., Olsen, E.M., Gothelf, K.V., 2008. J. Am. Chem. Soc. 130, 4256–4258.
Gai, P., Kong, X., Zhang, S., Song, P., Li, F., 2020. Chem. Commun. 56, 7116–7119.
Hu, J., Jiang, Y.Z., Wu, L.L., Wu, Z., Bi, Y., Wong, G., Qiu, X., Chen, J., Pang, D.W., Zhang, Z.L., 2017. Anal. Chem. 89, 13105–13111.
Hu, J., Liu, W., Wang, J., Qiu, J.G., Zhang, C.Y., 2021. Anal. Chem. 93, 6913–6918.
Hu, M., Yuan, C., Tian, T., Wang, X., Sun, J., Xiong, E., Zhou, X., 2020. J. Am. Chem. Soc. 142, 7506–7513.
Jing, W., Wang, Y., Yang, Y., Wang, Y., Ma, G., Wang, S., Tao, N., 2019. ACS Nano 13, 8609–8617.
Kelley, S.O., 2017. Acc. Chem. Res. 50, 503–507.
Li, L., Wang, L., Xu, Q., Xu, L., Liang, W., Li, Y., Ding, M., Aldalbahi, A., Ge, Z., Wang, L., 2018. ACS Appl. Mater. Interfaces 10, 6895–6903.
Long, G.L., Winefordner, J.D., 1983. Anal. Chem. 55, 712A–724A.
Miao, P., Tang, Y., 2021. ACS Cent. Sci. 7, 1036–1044.
Nesterova, I.V., Nesterov, E.E., 2014. J. Am. Chem. Soc. 136, 8843–8846.
Pei, H., Li, F., Wan, Y., Wei, M., Liu, H., Su, Y., Chen, N., Huang, Q., Fan, C., 2012. J. Am. Chem. Soc. 134, 11876–11879.
Shi, L., Mu, C., Gao, T., Chen, T., Hei, S., Yang, J., Li, G., 2018. Chem. Commun. 54, 11391–11394.
Shi, L., Sun, Y., Mi, L., Li, T., 2019. ACS Sens. 4, 3219–3226.
Somasundaram, S., Easley, C.J., 2019. J. Am. Chem. Soc. 141, 11721–11726.
Wang, C., Yu, P., Guo, S., Mao, L., Liu, H., Li, Y., 2016. Chem. Commun. 52, 5629–5632.
Wu, H., Qian, C., Wu, C., Wang, Z., Wang, D., Ye, Z., Ping, J., Wu, J., Ji, F., 2020. Biosens. Bioelectron. 157, 112153.
Xiao, T., Wu, F., Hao, J., Zhang, M., Yu, P., Mao, L., 2017. Anal. Chem. 89, 300–313.
Xue, Y., Wang, Y., Feng, S., Yan, M., Huang, J., Yang, X., 2021. Anal. Chem. 93, 8962–8970.
Yang, K., Wang, H., Ma, N., Zeng, M., Luo, H., He, D., 2018. ACS Appl. Mater. Interfaces 10, 44546–44553.
Ying, Z.M., Tu, B., Liu, L., Tang, H., Tang, L.J., Jiang, J.H., 2018. Chem. Commun. 54, 3010–3013.
Zhang, M., Wang, H., Wang, H., Wang, F., Li, Z., 2021. Anal. Chem. 93, 7942–7948.
Zhang, X., Song, C., Yang, K., Hong, W., Lu, Y., Yu, P., Mao, L., 2018. Anal. Chem. 90, 4968–4971.
Zhang, Y.J., Guo, L., Yu, Y.L., Wang, J.H., 2020. Anal. Chem. 92, 15699–15704.
Zhou, P., Gong, S., Liu, B., Shi, M., Lu, F., Li, N., Tang, B., 2021. Chem. Commun. 57, 6058–6061.
Zhu, D., Song, P., Shen, J., Su, S., Chao, J., Aldalbahi, A., Zhou, Z., Song, S., Fan, C., Zuo, X., 2016. Anal. Chem. 88, 4949–4954.
Zouari, M., Campuzano, S., Pingarrón, J.M., Raouafi, N., 2020a. Microchim. Acta 187, 1–11.
Zouari, M., Campuzano, S., Pingarrón, J.M., Raouafi, N., 2020b. Anal. Chim. Acta 1104, 188–198.